Published in final edited form as:
Circ Cardiovasc Imaging. 2018 November ; 11(11): . doi:10.1161/CIRCIMAGING.117.007453.

Simultaneous Assessment of Cardiac Inflammation and Extracellular Matrix Remodeling after Myocardial Infarction

Isabel T. Ramos, PhD[1,2], **Markus Henningsson, PhD**[1], **Maryam Nezafat, PhD**[1], **Begoña Lavin, PhD**[1,2], **Silvia Lorrio, PhD**[1,2], **Pierre Gebhardt, PhD**[1,3], **Andrea Protti, PhD**[1], **Thomas R. Eykyn, PhD**[1], **Marcelo E. Andia, MD, PhD**[4], **Ulrich Flögel, PhD**[5], **Alkystis Phinikaridou, PhD**[1,2], **Ajay M. Shah, MD, FMedSci**[2], and **René M. Botnar, PhD**[1,6]

[1]School of Biomedical Engineering and Imaging Sciences, King's College London, London, United Kingdom

[2]School of Cardiovascular Medicine and Sciences, King's College London British Heart Foundation Centre of Excellence, London, United Kingdom

[3]Department of Physics of Molecular Imaging Systems, Institute for Experimental Molecular Imaging, RWTH Aachen University, Aachen, Germany

[4]Radiology Department, School of Medicine, Pontificia Universidad Catolica de Chile, Santiago, Chile

[5]Department of Molecular Cardiology, Heinrich Heine University Duesseldorf, Duesseldorf, Germany

[6]Escuela de Ingeniería, Pontificia Universidad Católica de Chile, Santiago, Chile

Abstract

Background—Optimal healing of the myocardium following myocardial infarction (MI) requires a suitable degree of inflammation and its timely resolution, together with a well-orchestrated deposition and degradation of extracellular matrix (ECM) proteins.

Methods and Results—MI and SHAM-operated animals were imaged at 3,7,14 and 21 days with 3T magnetic resonance imaging (MRI) using a $^{19}F/^{1}H$ surface coil. Mice were injected with ^{19}F-perfluorocarbon (PFC) nanoparticles to study inflammatory cell recruitment, and with a gadolinium-based elastin-binding contrast agent (Gd-ESMA) to evaluate elastin content. ^{19}F MRI signal co-localized with infarction areas, as confirmed by late-gadolinium enhancement, and was highest 7days post-MI, correlating with macrophage content (MAC-3 immunohistochemistry) (ρ=0.89,*P<0.0001*). ^{19}F quantification with *in vivo* (MRI) and *ex vivo* nuclear magnetic resonance (NMR) spectroscopy correlated linearly (ρ=0.58,*P=0.020*). T_1 mapping after Gd-ESMA injection showed increased relaxation rate (R_1) in the infarcted regions and was significantly higher at 21days compared with 7days post-MI ($R_1[s^{-1}]$:21days=2.8 [IQR,2.69-3.30] vs 7days=2.3 [IQR, 2.12-2.5], *P<0.05*), which agreed with an increased tropoelastin content (ρ=0.89, *P<0.0001*). The

Correspondence: Isabel Maria da Silva Teixeira Ramos, PhD, School of Biomedical Engineering and Imaging Sciences, The Rayne Institute, 4th Floor, Lambeth Wing, St. Thomas' Hospital, London, SE1 7EH, United Kingdom, Tel: +44 20 718 88384, Fax: +44 20 718 85442, isabel.ramos@kcl.ac.uk.

Disclosures: None.

Europe PMC Funders Author Manuscripts

predictive value of each contrast agent for beneficial remodeling was evaluated in a longitudinal proof-of-principle study. Neither R_1 nor ^{19}F at day 7 were significant predictors for beneficial remodeling (*P=0.68*;*P=0.062*). However, the combination of both measurements (R_1<2.34Hz and 0.55≤^{19}F≤1.85) resulted in an odds ratio of 30.0 (CI95%:1.41-638.15;*P=0.029*) for favorable post-MI remodeling.

Conclusions—Multinuclear $^{1}H/^{19}F$ MRI allows the simultaneous assessment of inflammation and elastin remodeling in a murine MI model. The interplay of these biological processes affects cardiac outcome and may have potential for improved diagnosis and personalized treatment.

Journal Subject Terms

Magnetic Resonance Imaging (MRI); Inflammation; Ischemia; Fibrosis; Translational Studies

Keywords

magnetic resonance imaging; imaging; cardiac biomarkers; macrophage; extracellular matrix; molecular imaging; myocardial remodeling

Introduction

Cardiac injury activates innate immunity which initiates an inflammatory response whereby neutrophils and monocytes/macrophages are recruited to the myocardium 1. Immediately after MI, neutrophils are recruited to the site of injury, followed by the recruitment of monocytes/macrophages that remove dead cells and debris by phagocytosis 1,2. Studies have shown that an early and aggressive immune response and high levels of neutrophils and monocytes within the infarct may promote adverse remodeling and lead to poor prognosis 3,4. In addition to their phagocytic properties, inflammatory cells activate reparative pathways including the formation and deposition of scar tissue, which is mainly composed of collagen and elastin/tropoelastin 2,5,6. Elastin has been shown to be essential for the stabilization of the scar after MI and improving cardiac function by preserving elasticity 7,8. While the healthy myocardium contains elastin only to a negligible degree within the interstitium and coronary vasculature, an increase of elastic fibers within the myocardial scar is detected in the first weeks following ischemic injury developing a dense network between the remaining viable myocytes, myofibroblasts and smooth muscle cells during the maturation of the infarct 5. Tropoelastin, the soluble precursor of elastin, is synthetized in significant amounts and deposited within the remodeled myocardium, particularly at later stages of the healing process 9.

MRI has great potential to noninvasively assess both structure and function of the heart. By combining MRI with specific contrast agents, different biological processes can be targeted and tracked over time. In this study, we sought to explore the merits of multinuclear $^{1}H/^{19}F$ MRI for the sequential assessment and quantification of cardiac inflammation and elastin remodeling in a murine model of MI using a 3T clinical scanner. PFCs were used to assess inflammatory cell recruitment and Gd-ESMA was employed for the investigation of elastin deposition and quantification of ECM remodeling of the myocardium. This approach may potentially allow a more accurate characterization of early or persistent inflammation and

Europe PMC Funders Author Manuscripts

Europe PMC Funders Author Manuscripts

diffuse myocardial remodeling at the molecular level. It may also serve as a new biomarker for monitoring treatment response and evaluation of novel cardioprotective therapies.

Methods

The DICOM MR images will be made available to other researchers for purposes of reproducing the results 10.

Animal model

The institutional subcommittee on research animal care approved all animal studies. MI was induced in 10-week-old female C57BL/6J mice (n=71; 21% mortality rate) (Charles River, United Kingdom) by permanent occlusion of the left anterior descending coronary artery (LAD). Mice were anaesthetized by intraperitoneal injection of 75 mg/kg ketamine (Vetalar™V, Vetmedica, USA) and 1 mg/kg medetomidine hydrochloride (Domitor®, Orion Corporation, Finland). The animals underwent endotracheal intubation before surgery using an animal ventilator (Hugo Sacks Elektronic, Germany). A left thoracotomy was performed in the fourth intercostal space, the pericardium removed, and the LAD was permanently ligated with an 8-0 nylon suture (Direct Medical Supplies, Alton, UK). Successful ligation was confirmed by the regional blanching of the left-ventricle (LV), extending to the apex. After thoracotomy, subcutaneous tissue and skin were closed in separate layers and the animal was weaned from the ventilator. After the surgery, mice were monitored and maintained in a heated chamber for at least 6 h. Sham-operated animals underwent the same surgical procedure, without LAD ligation. Thirty minutes prior to recovery, 0.15 mg/kg buprenorphine (Vetergesic®, Alstoe, UK) was administered for analgesia by intramuscular injection.

Magnetic Resonance Imaging

In vivo cardiac scans were performed using a 3T Philips Achieva MR scanner (Philips Healthcare, Best, The Netherlands) equipped with a clinical gradient system (30 mT m^{-1}, 200 mT $m^{-1}(ms)^{-1}$). Mice (n=8 per time point) were imaged at 3, 7, 14 and 21 days post-MI. Sham-operated mice (n=6 per time point) were imaged at the same time points and were used as controls (Fig.1A). Fifteen mice were imaged longitudinally at 7 and 21 days post-MI (Fig.1B). Animals were placed in a prone position on a $^{19}F/^{1}H$ surface coil (Rapid Biomedical, Würzburg, Germany; diameter=23mm and 33mm). Anesthesia was induced with 5% and maintained with 1.5-2% isoflurane in medical oxygen during the MRI scan, and the body temperature was measured with a rectal temperature probe and maintained at 35±1°C using a water-based heating system (SA Instruments, Stony Brook, NY). ECG was monitored with two metallic needles placed subcutaneously in the region of the chest. ^{1}H and ^{19}F cardiac ECG-triggered MR images were acquired 48h after i.v. injection of 400μL of 10% perfluoro-15-crown-5 ether emulsion (PFC), as previously described 11 and 0.5mmol/kg of a gadolinium-based MRI contrast agent that targets elastin and tropoelastin, Gd-ESMA (Lantheus Medical Imaging, North Billerica, MA), administered 1h prior to the MRI scan. At the end of the scans, the mice were culled and the heart was extracted for histological and NMR studies.

Europe PMC Funders Author Manuscripts

After a 3-dimensional (3D) gradient echo scout scan, 2-dimensional (2D) cine short-axis images, covering the entire LV, were acquired to analyze functional and volumetric parameters. Imaging parameters were: FOV=35x35x12mm^3, acquired in-plane resolution=0.3x0.3x1mm^3, slices=12, TR/TE=7.8/16.0ms, flip angle=20°. Subsequently, a 2D Look-Locker scan planned perpendicular to the left-ventricle was used to determine the optimal inversion time (TI) for nulling of the healthy myocardium. 3D short-axis late-gadolinium-enhancement (LGE) gradient echo (GRE) images were acquired between 60-80min after Gd-ESMA injection for the visualization of contrast uptake within the infarcted region with the following parameters: FOV=35x35x12mm^3, acquired in-plane resolution=0.3x0.3x1mm^3, slices=12, TR/TE=6.4/2.6ms, 5 heart beats between subsequent IR pulses, and flip angle=25°. T_1-mapping was performed using a 2D Modified Look-Locker inversion recovery (MOLLI) sequence 12. The inversion pulse was followed by eight segmented readouts, each spaced one RR-interval apart, for eight individual images resulting in TI's ranging from 10ms to 2000ms. To allow full magnetization recovery, 12 pauses/heart beats were performed before the next inversion pulse. Acquisition parameters included: FOV=35x35x1.5mm^3, acquired in-plane resolution=0.3x0.3mm^3, slices=1, TR/TE=7.5/3.1ms, flip angle=16°. For the visualization of the inflammatory cells, a 3D turbo-spin echo ^{19}F scan was acquired with a FOV=35x35x12mm^3, acquired in plane resolution=1x1x2mm^3, slices=12, TR/TE=4beats/8.9ms, TSE factor=5, offset frequency=10200Hz (BW=6103Hz). A saturation slice was used to suppress the liver signal. To enable SNR calculation, a noise-scan was acquired with the same imaging parameters but without any RF pulses to correct for local noise variability. A T_2-weighted sequence was used to analyze edema within the heart at 3 and 7 days post-MI, with the following parameters: FOV=35x35x1.5mm^3, acquired in-plane resolution=0.3x0.3mm^2, slices=3, TR/TE=126/18ms, flip angle=30°.

Magnetic resonance image analysis

Ejection fraction (EF, %), left ventricular end-diastolic volume (LVEDV, μl) and left-ventricular mass (LV, mg) were calculated from the cine images, using an automated segmentation software (ClinicalVolumes, King's College London, www.clinicalvolumes.com) 13. Total infarct size was calculated by adding the LGE measured on consecutive slices after the administration of Gd-ESMA (LGE-ESMA). The sum of the total infarcted area was multiplied by the slice thickness to generate a volume (mm^3) and was then divided by the total LV myocardium and expressed as percentage. T_1 relaxation times (R_1) were calculated by manually segmenting T_1 map regions corresponding to the LGE-ESMA using OsiriX (Osirix Foundation, Geneva, Switzerland). For ^{19}F measurements, regions of interest were defined as areas of enhancement seen on the LGE-ESMA images. For these areas, ^{19}F signal was calculated using the following equation: $^{19}F\ signal = \frac{\sum SNR}{scar\ volume}$, where SNR is the sum of the signal of the infarcted area divided by the standard deviation of the noise in each slice, and scar volume was calculated from the sum of the LGE-ESMA area of each slice multiplied by the MRI slice thickness 14.

Nuclear magnetic resonance spectroscopy

Nuclear magnetic resonance (NMR) spectroscopy was used to quantify the uptake of PFC *ex vivo*. Mice injected with PFC and scanned at 3T were culled and the hearts were collected (MI: n=4 and SHAM: n=3; each per time point). Remote and infarcted regions were separated, weighed and frozen at -20°C prior to NMR analysis. NMR spectra of the PFCs were recorded at room temperature using a Bruker Avance III 9.4T scanner (^{1}H 400MHz; ^{19}F 375.8MHz) and a 15-mm-diameter-large, double-tuned (^{31}P/^{1}H) volumetric micro-imaging coil. The water resonance was used to shim the sample and the ^{1}H coil was then re-tuned to the ^{19}F frequency. Both remote and infarcted areas were placed in NMR tubes (Fisher Scientific, Leicestershire, UK) with a silicone support to position the sample within the isocentre of the coil. A sealed external reference capillary of 100% TFA solution (δTFA=-76.6ppm as identified in the literature, and reported relative to $CFCl_3$) was placed adjacent to the heart. The ^{19}F NMR chemical shift of the PFC peak was -12.5ppm relative to the reference capillary. A 90° RF pulse (30μs hard pulse) was used together with a number of signal averages=64, total experiment duration=4.78min, time domain size=131K data points, pre-scan delay=1s, acquisition time=3.5s to give a total repetition time of TR=4.5s per scan, spectral bandwidth=18797Hz. Data were processed with an exponential line broadening factor (20Hz), followed by Fourier transformation, zero and first order phase correction and automatic baseline correction. Peaks corresponding to the TFA reference and the PFC were integrated using Topspin 2.1 software (Bruker Biospin GmbH, Rheinstetten Germany) and normalized to the reference capillary. The number of moles of ^{19}F were calculated using the equation: $[PFC] = \frac{N_{TFA} \times I_{PFC} \times [TFA]}{N_{PFC} \times I_{TFA} \times g_{tissue}}$ where [PFC] is the concentration/g tissue (wet weight)), N_{TFA} is the number of ^{19}F nuclei giving rise to the TFA signal, N_{PFC} is the number of ^{19}F nuclei giving rise to the PFC signal, I_{PFC} is the peak integral of the PFC peak, I_{TFA} is the peak integral of the TFA peak (I_{TFA}=1, normalized), [TFA] is the number of moles of TFA.

Histology

Following the MRI scans, anesthetized mice were culled by neck dislocation and hearts were collected for *ex vivo* analysis (n=4 MI mice per time point, and n=3 SHAM-operated animals per time point). Hearts were harvested, the atriums were removed and the ventricles were washed in saline solution followed by immersion in 10% formaldehyde solution for 24h at room temperature. Hearts were then dehydrated, paraffin-embedded and transversely sectioned (5μm thick).

Immunohistochemistry (IHC) was used to quantify the amount of tropoelastin and macrophages in the myocardium. Tropoelastin was detected with anti-mouse rabbit polyclonal antibody (21600, Abcam; dilution 1:100) using an avidin-biotin-peroxidase method (Vector® SG Peroxidase substrate; Vector Laboratories, Burlingame, CA). A monoclonal rat anti-mouse antibody (550292, BD Pharmingen) (CD107b; MAC-3; dilution 1:100) was used for macrophage detection. The antibody was revealed with streptavidin-peroxidase (Dako, Ely, UK) (ABC kit, 1:100). Digital images were analyzed using ImageJ (National Institute of Health, Bethesda, MD). Tropoelastin and MAC-3 were quantified and expressed as percentage of the infarcted myocardium using ImageJ, and were manually

segmented and normalized with the total area of infarction for each histology slice calculated from Masson's trichrome staining.

Statistical analysis

GraphPad Prism 5.00 (GraphPad Software, Inc., La Jolla, California, USA) was used for statistical analysis. Nonparametric exact tests were used for analysis. Differences between different time-point measurements were analysed using Kruskal-Wallis test for multiple group comparisons, and if this test was significant, it was followed by Dunn's post-hoc test. Differences between different time-points and different groups: SHAM/scar/remote were analysed using a two-way ANOVA. Correlations were assessed using Spearman rank test. In order to study the non-linear behaviour of ^{19}F in the longitudinal study, the linear correlation model was compared with second order polynomial model regression; both variables (EDV at day 21 and ^{19}F SNR) were first tested for normal distribution using the D'Agostino-Pearson omnibus normality test. Receiver operating characteristic (ROC) curve analysis was performed to identify the cut-off point of imaging biomarkers to predict the evolution of functional cardiac parameters; in this case, the increase in the end diastolic left ventricle volume (EDV) between day 7 and day 21 was considered as dysfunctional remodeling, and the decrease of EDV between day 7 and day 21 was considered as a beneficial remodeling. $P<0.05$ was considered statistically significant. Data are presented as median, and interquartile range.

Results

Assessment of Cardiac Function by MRI at 3T

Cardiac function was assessed using cine MRI and results are summarized in Figure 2 (detailed results in supplement Table S1). A visual enlargement of the left ventricle and thinning of the ventricular wall at the site of the infarction, was observed post-MI and became more evident at day 21. These results are consistent with previous studies in the same animal model 15.

Assessment of the inflammatory response in post-MI remodeling using PFCs

Myocardial remodeling post-MI is associated with an acute inflammatory response. Combined proton (^{1}H) and fluorine (^{19}F) images confirmed co-localization of the PFCs within the infarcted area at both 3 and 7 days (Fig.3A).

Quantitative *in vivo* ^{19}F MRI showed a significant increase of ^{19}F signal (SNR/scar volume) within the infarcted area at 7 days post-MI (SNR=1.27 [IQR, 0.84-1.58]) compared with SHAM-operated animals (SNR=0.19 [IQR, 0.13-0.20], $P<0.001$) (Fig.3B). A maximum ^{19}F signal was observed at 7 days post-MI which was significantly greater than at 3 days (SNR=0.44 [IQR, 0.39-0.67], $P<0.05$), 14 days (SNR=0.30 [IQR, 0.23-0.34], $P<0.01$). At 21 days post-MI (SNR=0.18 [IQR, 0.15-0.28] the ^{19}F signal was negligible and significantly lower compared to 3 days ($P<0.05$) and 7 days ($P<0.001$), consistent with the resolution of inflammation. ^{19}F signal was also detected at the site of thoracotomy, in the liver and lymph nodes, as these are major sites of macrophage clearance. Although the spleen was outside

Europe PMC Funders Author Manuscripts

our imaging volume, PFC uptake would be also expected in this organ (as seen by other studies) 16.

To verify the *in vivo* results and to quantify the evolution of the ^{19}F signal, infarcted and remote areas were dissected and separated for *ex vivo* NMR spectroscopy acquired on whole tissue samples. NMR spectra were in good agreement with the *in vivo* MRI findings, where infarcted regions showed high PFC signal that was absent in the remote myocardium (Fig. 3C). NMR analysis showed a maximum ^{19}F concentration (mmol/g tissue) at 7 days post-MI ([^{19}F]=0.12 [IQR, 0.075-0.18], *P<0.05*) that was significantly higher compared with 21 days post-MI ([^{19}F]=0.0063 [IQR, 0.0042-0.020]). At 7 days post-MI the uptake in the region of infarcted myocardium was significantly greater than both remote myocardium ([^{19}F]=0.026 [IQR, 0.015-0.057], *P<0.05*) and healthy hearts from SHAM-operated animals ([^{19}F]=0.012 [IQR, 0.0042-0.044], *P<0.05*). At 21 days post-MI, the signal in the remote myocardium was statistically different from SHAM-operated animals. In SHAM-operated animals injected with PFC, no ^{19}F signal was detected in the heart. A linear correlation was observed between *in vivo* MRI measurements and *ex vivo* NMR ^{19}F signal measurements (ρ=0.58, *P=0.020*, Fig.S1).

MAC-3 IHC for identification of myocardial tissue macrophages showed recruitment of these cells into the infarcted area at the early stages following MI but not to the remote myocardium as seen by *in vivo* imaging (Fig.3A). The number of MAC-3 positive macrophages was significantly higher at 3 days post-MI ($IHC_{MAC\text{-}3}$[%]=2.12 [IQR, 1.88-2.63], *P<0.05*) and 7 days post-MI ($IHC_{MAC\text{-}3}$[%]=3.65 [IQR, 2.74-4.09], P *<0.01*) compared with SHAM animals ($IHC_{MAC\text{-}3}$[%]=0.003 [IQR, 0.002-0.004]) and was significantly higher at 7 days post-MI compared to 21 days post-MI ($IHC_{MAC\text{-}3}$[%]=0.13 [IQR, 0.041-0.23], *P<0.05*) (Fig.3D). There was a significant correlation between the *in vivo* ^{19}F MRI signal and macrophage content as quantified by IHC (ρ=0.89, *P<0.0001*, Fig.3E).

Assessment of elastin remodeling post-MI using Gd-ESMA

ECM remodeling post-MI was evaluated using Gd-ESMA, a contrast agent that binds to both cross-linked elastin and immature tropoelastin 17,18. One hour post-Gd-ESMA injection, infarcted areas were enhanced at all time-points post-MI, allowing quantification of infarct size. Trichrome staining was performed and used to quantify infarct size *ex vivo*. There was a strong linear correlation between infarct size measured by *in vivo* MRI and histology (ρ=0.85, *P<0.0001*) (Fig.S2).

To understand the contribution of fluid accumulation in the interstitial space to the MR signal early after MI, myocardial edema was assessed using a T_2W sequence 19–21. High signal was observed at day 3 but not at day 7 post-MI. The signal intensity seen on T2W images at day 3 was associated with edema and increased extracellular volume, but did not reflect deposition of elastin/tropoelastin as confirmed by histology (Figure 4).

In-vivo quantification of Gd-ESMA uptake was performed using a MOLLI T_1 mapping sequence. Relaxation rate (R_1) maps showed uptake of Gd-ESMA in the infarcted area (increased R_1) at 3, 7, 14 and 21 days post-MI while no enhancement was observed in the remote myocardium (infarct vs remote, *P<0.01*, Fig.5B) nor in the SHAM-operated animals

(infarct vs SHAM, *P<0.001*, Fig.5B). R_1 values were also significantly higher within the infarct area at 21 days ($R_1[s^{-1}]$=2.83 [IQR, 2.69-3.30], *P<0.05*) compared to 7 days ($R_1[s^{-1}]$=2.3 [IQR, 2.12-2.5]).

To analyze the deposition of elastin fibers in the heart after MI, Elastica van Gieson staining was performed. Mature fibers could be visualized, however, quantification was challenging (Fig.S3). For that reason, tropoelastin IHC was performed (Fig.5A&C) revealing a dense fiber network within the infarcted myocardium at 14 and 21 days post-MI but not in the remote myocardium. Tropoelastin deposition was significantly higher at both 14 days [$IHC_{Tropoelastin}$[%]=2.78 [IQR, 2.51-3.07] and 21 days ($IHC_{Tropoelastin}$[%]=3.25 [IQR, 2.87-3.45]) compared to SHAM ($IHC_{Tropoelastin}$[%]=0.14 [IQR, 0.13-0.15], *P<0.01*). For the reason abovementioned, the three days' time-point was excluded from the correlation analysis between R_1 and tropoelastin IHC analyses. There was a statistically significant correlation between R_1 values from 7, 14 and 21 days measured *in vivo* and *ex vivo* IHC analysis (ρ=0.89, *P<0.0001*, Fig.5D).

^{19}F vs R_1 can be used to predict cardiac remodeling: longitudinal study

Remodeling post-MI is a dynamic and complex process. To understand the potential prognostic value of *in vivo* ^{19}F and Gd-ESMA MRI, a longitudinal proof-of-principle study was performed. Fifteen animals were scanned twice at days 7 and 21 post-MI. ^{19}F MRI was performed at 7 days post-MI to assess the peak in the inflammatory response and MRI with Gd-ESMA was performed at days 7 and 21 post-MI. No correlation was found between ^{19}F at day 7 post-MI and Gd-ESMA uptake at day 7 (Fig.6A) and at day 21 post-MI (Fig.6B), suggesting that these biological processes are independent/decoupled from each other.

The presence of elastin at day 7 (measured as R_1) showed a linear correlation with the EDV measured at day 21, suggesting that early accumulation of elastin/tropoelastin (larger Gd-ESMA uptake at day 7) might not be beneficial for the healing of the myocardium at day 21 (Fig.7A). In contrast, the inflammatory process measured at day 7 showed a more complex behaviour (second order polynomial model regression showed significant correlation than the linear model (*P=0.030*). PFCs data suggest that an optimal inflammatory response was observed for a ^{19}F signal range between 0.55 and 1.85. Both an increased ($^{19}F>>1.85$) or weak ($^{19}F<<0.55$) inflammatory response at early stages post-MI resulted in large EDV (EDV>100μl) at day 21 suggesting adverse cardiac outcome (Fig.7B).

The prognostic value of the ^{19}F signal (^{19}F SNR) and quantitative assessment of elastin/tropoelastin deposition (R_1) was investigated with ROC analysis (Fig.S4). Both measurements carry some predictive value ($R_1<2.34$: [Sens(%) + IC95%]=54.5 (22.0-87.0), [Specif(%) + IC95%]=100 (92.1-100.0); $0.55<{}^{19}F<1.85$: [Sens(%) + IC95%]=50 (20.5-79.5), [Specif(%) + IC95%]=82 (59.3-100.0)) but the combination of both improved the sensitivity and specificity in identifying animals that underwent favorable myocardial remodeling post-MI ($R_1<2.34$ and $0.55<{}^{19}F<1.85$: [Sens(%) + IC95%]=75 (49.4-100.0), [Specif(%) + IC95%]=91 (74.1-100.0)). Logistic regression analysis using the increase of EDV at day 21 (dysfunctional remodeling) or the decrease of EDV at day 21 (beneficial remodeling) as outcome result, showed that R_1 at day 7 and ^{19}F at day 7 were not significant

predictors by themselves (*P=0.68* and *P=0.062* respectively). However, the combination of both measurement results in an OR of 30.0 (CI95%: 1.41-638.15), *P=0.029*.

Discussion

In this cross-sectional study we showed that 1) PFCs ^{19}F MRI can be used to assess and monitor inflammatory cell recruitment *in vivo* in the injured myocardium at a clinical field strength, as confirmed by *ex vivo* NMR and histological studies; 2) Gd-ESMA MRI allows quantification and visualization of scar size and elastin/tropoelastin deposition in the myocardium during the scar maturation phase. 3) In a longitudinal proof-of-concept study, we further investigated the merits of both biomarkers for the prediction of the amount of cardiac remodeling (measured as EDV). We found that at the early stages post-MI a weak or strong inflammatory response results in dysfunctional MI healing, and that increased elastin/tropoelastin deposition within the scar tissue at the 7 day's time-point is detrimental for cardiac remodeling. Our results suggest that multinuclear ^{19}F/^{1}H MRI may provide a better understanding of the biological processes underlying post-MI remodeling *in vivo* and PFCs and Gd-ESMA may serve as new imaging biomarkers for monitoring the progression of cardiac disease and allow predicting outcome.

Within the first week after MI inflammatory cells are recruited to the site of injury. Phagocytes avidly take up PFCs, which can be imaged by ^{19}F MRI with excellent contrast and without unwanted background signal, as shown previously 11,14,22,23. However, no study has described the temporal evolution of ^{19}F signal *in vivo* at clinical field strength. Here we investigated the time course of inflammation using PFCs *in vivo* in a model of MI and related with the presence of immune cells. We successfully demonstrated the non-invasive visualization and quantification of inflammatory cells with PFCs in the infarcted region in a murine model of MI by *in vivo* MRI, validated *ex vivo* by NMR. MRI signal intensity measurements demonstrated that ^{19}F is detectable within the first week post-MI, with a peak at 7 days, and importantly, PFC accumulation was restricted only to the infarcted region. Consistent with these findings, histological analysis showed that monocyte/macrophage populations are significantly increased up to 7 days after LAD occlusion as detected by immune positive MAC-3 staining and, furthermore, we found a strong correlation between MAC-3 and ^{19}F MRI signal. Our results are also in good agreement with the resolution of inflammatory response at days 14 and 21 as described in animal models of MI 2,24,25.

Non-invasive imaging of inflammatory cells recruitment to the injured and remote myocardium has been shown by PET *in vivo* 26 but requires special patient preparation to suppress myocardial glucose metabolism. Alternatively, magnetic nanoparticles (MNP) have been used for macrophage imaging post *MI in vivo* 27; however, despite their excellent sensitivity, they generate negative contrast due to shortened T2/T2* relaxation times of nearby water protons, creating hypointense regions and consequently making quantification challenging. Moreover, MNPs cannot be used in combination with other Gd-based contrast agents. In contrast, PFCs are detected directly and therefore generate positive signal contrast, and more importantly can be imaged simultaneously with e.g. Gd-based contrast agents affecting only the extracellular ^{1}H signal whilst ^{19}F PFCs will be located

Europe PMC Funders Author Manuscripts

intracellularly following phagocytosis. The potential of ^{19}F particles has been extensively explored in preclinical models; they are chemically stable and can be further functionalized by adding fluorochromes, thus allowing multimodal imaging (e.g. MRI and fluorescence imaging). In this work, we did not investigate if PFCs can differentiate between the monocyte/macrophage sub-populations ($Ly6C^{high}$ vs $Ly6C^{low}$; M1 vs M2) during post-MI remodeling *in vivo*, which would be of great interest. Previous publications have suggested the recruitment of macrophages to the remote myocardium 26,27; here, due to sensitivity we could not detect myocardial leukocyte enrichment. Nevertheless, ^{19}F MRI may provide an *in vivo* readout for monitoring treatment-related changes in total inflammatory cell infiltration.

As the inflammatory process dissipates, fibrotic tissue accumulates in the infarcted regions and is then replaced by ECM proteins. Scar tissue formation commences as early as 1 week post-MI, and is mainly composed of collagen type I but also elastin. Elastin is an insoluble protein that has been associated with scar formation and stabilization 8,28,29. Mature elastin is formed by cross-linking of its soluble precursor, tropoelastin. Here, we took advantage of the increasing expression of elastin/tropoelastin during post-MI remodeling and investigated the use of Gd-ESMA as an imaging biomarker for the assessment of ECM remodeling. Elastin/tropoelastin was quantified using T_1 mapping to measure relaxation rates (R_1) after Gd-ESMA injection with 3T MRI. R_1 values significantly increased from 7 to 21 days post-MI, which was in good agreement with the deposition of tropoelastin in the infarcted area measured by histology. At 3 days post-MI, T_1 mapping showed a significant increase in R_1 in the infarcted area, however histology showed a lack of elastin/tropoelastin at this time-point. We hypothesized that Gd-ESMA acts similarly to other gadolinium-based contrast agents due to its small size 17,30, and immediately after MI its retention within the infarcted region may be unspecific and attributed to edema, cellular swelling and rupture, and subsequent increase in extracellular volume, as previously shown in dogs and humans 19–21. Consistent with this hypothesis, we observed a high signal intensity on native T_2W images at day 3 (high water content) in the infarcted area, which decreased at day 7 post-MI. Additionally, Gd-ESMA not only binds to tropoelastin and elastin (41%, K_D=9.2±0.7μM and 40%, K_D=1.0±0.5μM, respectively) but also to other proteins including BSA (15%, K_D=ns) and chondroitin sulfates (5%, K_D=ns) 31, collagen type I and III (22%, K_D=7.3±1.3μM and 13%, K_D=6.8±1.2μM, respectively) 18 that might be present at day 3, thus increasing its retention and tissue relaxation.

Gd-ESMA has been successfully used for molecular imaging of vessel wall elastin in atherosclerosis (30–32), and myocardial scar 15. ECM remodeling could also be assessed with alternative contrast agents specific for other matrix proteins such as collagen thereby providing additional biological information in addition to standard LGE MRI.

The recovery of cardiac function following MI is highly dependent on a balanced inflammatory response and on the deposition of ECM proteins within the heart. In our longitudinal proof-of-principle study the impact of the inflammatory response on LV remodeling was evaluated with PFCs and ECM remodeling with Gd-ESMA MRI. A moderate inflammatory response at day 3 (intermediate ^{19}F signal) was associated with a better LV remodeling at day 21 (measured as EDV). The healing process is affected by the exposure and duration of acute inflammation. Prolonged and exacerbated inflammation has

been related to worse prognosis and similarly, the lack of inflammation has been associated with thinner infarcts, where the myocardium is more likely to rupture 3,4. A certain degree of inflammation and a controlled recruitment of monocyte/macrophages populations seems to be desired for optimal MI healing. Likewise, Sahul *et al* 33 have shown that moderate amounts of metalloproteinases (MMPs) in the infarcted region lead to lower LV remodeling in a pig model of MI. Inflammatory cell migration towards the infarct requires the presence of MMPs to facilitate migration. Interestingly, while MMPs are crucial for the recruitment of inflammatory cells, this study has shown that excessive MMPs activation lead to LV expansion.

Here, we also have shown that higher R_1 values at 7 days (high elastin/tropoelastin deposition) were associated with an unfavorable prognosis at 21 days post-MI (high EDV). In previous work, Gd-ESMA has also been used to assess elastin deposition in the heart in a mouse model of MI. In their cross-sectional study, Wildgruber et al 17 found that a higher CNR between scar and remote myocardium at day 21 correlated with a higher EF at the same time-point, while the CNR at day 7 did not predict outcome at day 21. In contrast, we performed a longitudinal study, using T_1 mapping and EDV as a readout for LV remodeling. Other studies showed that modifying the composition of myocardial scar by exogenously increasing elastin content, cardiac function was improved after MI in rats 7–9. Also, increased expression of elastin via cell-based gene therapy improved cardiac function and survival of ischemic hearts in a rat model of MI 8,34. Further studies are needed to pinpoint the long-term role of elastin turnover/metabolism and cross-linking following MI.

Finally, we have also shown that the combination of the R_1 at day 7 and ^{19}F at day 7 could predict the beneficial or dysfunctional LV remodeling, even though the OR is statistically significant, it has a wide confidence interval, which reflex the complex process of inflammation and remodeling, further studies, including bigger sample size and different animal models have to be used in order to validate this conclusion.

Overall, multinuclear $^{19}F/^{1}H$ MRI may improve our knowledge of cardiac remodeling *in-vivo* by targeting key biological processes that are responsible for post-MI remodeling. This imaging protocol may be useful for risk stratification or to facilitate the *in-vivo* study of the effects of novel therapeutic procedures in disease progression and potentially personalization of therapy.

Limitations

This study has shown the feasibility of multinuclear imaging in a murine model of post-MI remodelling via LAD ligation. ^{19}F imaging was performed in a small animal model using a clinical 3T MR scanner, where high amounts of PFCs (i.e. 3 mmol PFC per kg body weight) are required to generate enough signal. The high dosage enabled visualization of PFCs in small structures such as the murine heart. For early time-points ^{19}F deposition co-localized with LGE-ESMA enhancement within the scar area, however for days 14 and 21 LGE-ESMA images were used as guide for the analysis of PFC uptake. Direct quantification of PFCs from the MRI could not be performed, as a surface coil was used. However, with the use of NMR experiments at 9.4T we were able to quantify PFCs content both in the remote

Europe PMC Funders Author Manuscripts

and infarcted myocardium *ex vivo*. As PFCs used in this study were not specific for macrophages, signal accumulation in the infarct area might also be due to other cells with phagocytic capacity. PFC accumulation is not specific for myocardial inflammation but can also occur at other sites of inflammation (thoracotomy) and organs with high amounts of inflammatory and phagocytic cells such as the liver and lymph nodes. The here employed PFCs did not allow to differentiate between the monocyte/macrophage sub-populations ($Ly6C^{high}$ vs $Ly6C^{low}$; M1 vs M2) during post-MI remodeling *in vivo*. PFC injection did not show any adverse effects in the animals throughout the period of time animals were monitored. However, PFCs have long retention time in the body, making it challenging to obtain approval for clinical application. Further, improvement of the PFC nanoparticles biodistribution properties while maintaining their specificity for macrophages could aid future use in humans. Additionally, in our study we used a higher the dose of Gd-ESMA (0.5 mmol/kg) compared with that used in other animal models (0.2 mmol/kg) or non-targeted gadolinium-based agents in clinical studies. Future experiments will require dose optimization in myocardial infarction models or humans; however, no toxic effects have been observed in the animals at any time point. Finally, we utilised a permanent LAD occlusion model demonstrating a strong acute inflammatory response for proof-of-concept $^{19}F/^{1}H$ MRI of myocardial inflammation and remodelling after MI. In future studies, a reperfusion model will be investigated, as it is more clinically relevant. The permanent LAD occlusion model only produces a mild inflammatory response while the reperfusion model typically results in a stronger inflammatory response. Even though the inflammatory response was weaker in our model we were able to detect and quantify both inflammation and ECM deposition in the infarct zone, making these contrast agents promising biomarkers for future studies.

Conclusions

We successfully demonstrated the feasibility of multinuclear $^{1}H/^{19}F$ MRI to non-invasively assess and quantify the inflammatory response and evaluate elastin formation following post-MI remodeling in a murine model *in vivo*. We further studied the interplay between these biological processes and correlated those with LV remodeling. This novel approach has potential for monitoring treatment effects that aim to modulate the inflammatory or elastin responses *in vivo* and may aid the prognosis of cardiovascular diseases.

Supplementary Material

Refer to Web version on PubMed Central for supplementary material.

Sources of Funding

This work was supported by a King’s College London British Heart Foundation Centre of Excellence inter-disciplinary PhD fellowship, a British Heart Foundation Program grant (RG/12/1/29262) and the Wellcome Trust / EPSRC Centre for Medical Engineering (NS/A000049/1 and WT 203148/Z/16/Z).

References

1. Frangogiannis NG. The inflammatory response in myocardial injury, repair, and remodelling. Nat Rev Cardiol. 2014; 11:255–65. [PubMed: 24663091]

Europe PMC Funders Author Manuscripts

2. Frangogiannis NG. Regulation of the inflammatory response in cardiac repair. Circ Res. 2012; 110:159–73. [PubMed: 22223212]
3. Pfeffer MA, Braunwald E. Ventricular remodeling after myocardial infarction. Experimental observations and clinical implications. Circulation. 1990; 81:1161–72. [PubMed: 2138525]
4. Solomon SD, Glynn RJ, Greaves S, Ajani U, Rouleau JL, Menapace F, Arnold JM, Hennekens C, Pfeffer MA. Recovery of ventricular function after myocardial infarction in the reperfusion era: the healing and early afterload reducing therapy study. Ann Intern Med. 2001; 134:451–8. [PubMed: 11255520]
5. Bassett EG, Wakefield JS. Elastic fibers in myocardial scars in rats: development teraction with other components. Connect Tissue Res. 2008; 49:321–7. [PubMed: 18991085]
6. Whittaker P, Boughner DR, Kloner RA. Role of collagen in acute myocardial infarct expansion. Circulation. 1991; 84:2123–34. [PubMed: 1934383]
7. Mizuno T, Mickle DA, Kiani CG, Li RK. Overexpression of elastin fragments in infarcted myocardium attenuates scar expansion and heart dysfunction. Am J Physiol Heart Circ Physiol. 2005; 288:H2819–27. [PubMed: 15681698]
8. Mizuno T, Yau TM, Weisel RD, Kiani CG, Li RK. Elastin stabilizes an infarct and preserves ventricular function. Circulation. 2005; 112:I81–8. [PubMed: 16159870]
9. Lichtenauer M, Mildner M, Baumgartner A, Hasun M, Werba G, Beer L, Altmann P, Roth G, Gyöngyösi M, Podesser BK, Ankersmit HJ. Intravenous and intramyocardial injection of apoptotic white blood cell suspensions prevents ventricular remodelling by increasing elastin expression in cardiac scar tissue after myocardial infarction. Basic Res Cardiol. 2011; 106:645–55. [PubMed: 21416207]
10. Ramos IT, Henningsson M, Nezafat M, Lavin B, Lorrio S, Gebhardt P, Protti A, Eykyn TR, Andia ME, Flogel U, Phinikaridou A, et al. Simultaneous Assessment of Cardiac Inflammation and Extracellular Matrix Remodeling After Myocardial Infarction. figshare. 2018; doi: 10.6084/m9.figshare.5968963
11. Flögel U, Ding Z, Hardung H, Jander S, Reichmann G, Jacoby C, Schubert R, Schrader J. In vivo monitoring of inflammation after cardiac and cerebral ischemia by fluorine magnetic resonance imaging. Circulation. 2008; 118:140–8. [PubMed: 18574049]
12. Nezafat M, Ramos IT, Henningsson M, Protti A, Basha T, Botnar RM. Improved segmented modified Look-Locker inversion recovery T1 mapping sequence in mice. PLoS One. 2017; 12:e0187621. [PubMed: 29121086]
13. Protti A, Sirker A, Shah AM, Botnar R. Late gadolinium enhancement of acute myocardial infarction in mice at 7T: cine-FLASH versus inversion recovery. J Magn Reson Imaging. 2010; 32:878–86. [PubMed: 20882618]
14. Ebner B, Behm P, Jacoby C, Burghoff S, French BA, Schrader J, Flögel U. Early assessment of pulmonary inflammation by 19F MRI in vivo. Circ Cardiovasc Imaging. 2010; 3:202–10. [PubMed: 20061515]
15. Protti A, Lavin B, Dong X, Lorrio S, Robinson S, Onthank D, Shah AM, Botnar RM. Assessment of Myocardial Remodeling Using an Elastin/Tropoelastin Specific Agent with High Field Magnetic Resonance Imaging (MRI). J Am Heart Assoc. 2015; 4:e001851. [PubMed: 26272655]
16. Jacoby C, Temme S, Mayenfels F, Benoit N, Krafft MP, Schubert R, Schrader J, Flögel U. Probing different perfluorocarbons for in vivo inflammation imaging by 19F MRI: image reconstruction, biological half-lives and sensitivity. NMR Biomed. 2014; 27:261–71. [PubMed: 24353148]
17. Wildgruber M, Bielicki I, Aichler M, Kosanke K, Feuchtinger A, Settles M, Onthank DC, Cesati RR, Robinson SP, Huber AM, Rummeny EJ, et al. Assessment of myocardial infarction and postinfarction scar remodeling with an elastin-specific magnetic resonance agent. Circ Cardiovasc Imaging. 2014; 7:321–9. [PubMed: 24363356]
18. Botnar RM, Wiethoff AJ, Ebersberger U, Lacerda S, Blume U, Warley A, Jansen CH, Onthank DC, Cesati RR, Razavi R, Marber MS, et al. In vivo assessment of aortic aneurysm wall integrity using elastin-specific molecular magnetic resonance imaging. Circ Cardiovasc Imaging. 2014; 7:679–89. [PubMed: 24871347]

19. Abdel-Aty H, Cocker M, Meek C, Tyberg JV, Friedrich MG. Edema as a very early marker for acute myocardial ischemia: a cardiovascular magnetic resonance study. J Am Coll Cardiol. 2009; 53:1194–201. [PubMed: 19341860]
20. Dall'Armellina E, Karia N, Lindsay AC, Karamitsos TD, Ferreira V, Robson MD, Kellman P, Francis JM, Forfar C, Prendergast BD, Banning AP, et al. Dynamic changes of edema and late gadolinium enhancement after acute myocardial infarction and their relationship to functional recovery and salvage index. Circ Cardiovasc Imaging. 2011; 4:228–36. [PubMed: 21447711]
21. Willerson JT, Scales F, Mukherjee A, Platt M, Templeton GH, Fink GS, Buja LM. Abnormal myocardial fluid retention as an early manifestation of ischemic injury. Am J Pathol. 1977; 87:159–88. [PubMed: 139829]
22. Flögel U, Su S, Kreideweiss I, Ding Z, Galbarz L, Fu J, Jacoby C, Witzke O, Schrader J. Noninvasive detection of graft rejection by in vivo (19) F MRI in the early stage. Am J Transplant. 2011; 11:235–44. [PubMed: 21214858]
23. Temme S, Bönner F, Schrader J, Flögel U. 19F magnetic resonance imaging of endogenous macrophages in inflammation. Wiley Interdiscip Rev Nanomed Nanobiotechnol. 2012; 4:329–43. [PubMed: 22354793]
24. Frangogiannis NG. Targeting the inflammatory response in healing myocardial infarcts. Curr Med Chem. 2006; 13:1877–93. [PubMed: 16842199]
25. Jaffer FA, Sosnovik DE, Nahrendorf M, Weissleder R. Molecular imaging of myocardial infarction. J Mol Cell Cardiol. 2006; 41:921–33. [PubMed: 17067633]
26. Lee WW, Marinelli B, van der Laan AM, Sena BF, Gorbatov R, Leuschner F, Dutta P, Iwamoto Y, Ueno T, Begieneman MP, Niessen HW, et al. PET/MRI of inflammation in myocardial infarction. J Am Coll Cardiol. 2012; 59:153–63. [PubMed: 22222080]
27. Alam SR, Shah AS, Richards J, Lang NN, Barnes G, Joshi N, MacGillivray T, McKillop G, Mirsadraee S, Payne J, Fox KA, et al. Ultrasmall superparamagnetic particles of iron oxide in patients with acute myocardial infarction: early clinical experience. Circ Cardiovasc Imaging. 2012; 5:559–65. [PubMed: 22875883]
28. Yanagisawa H, Davis EC, Starcher BC, Ouchi T, Yanagisawa M, Richardson JA, Olson EN. Fibulin-5 is an elastin-binding protein essential for elastic fibre development in vivo. Nature. 2002; 415:168–71. [PubMed: 11805834]
29. Kielty CM, Sherratt MJ, Shuttleworth CA. Elastic fibres. J Cell Sci. 2002; 115:2817–28. [PubMed: 12082143]
30. Makowski MR, Wiethoff AJ, Blume U, Cuello F, Warley A, Jansen CH, Nagel E, Razavi R, Onthank DC, Cesati RR, Marber MS, et al. Assessment of atherosclerotic plaque burden with an elastin-specific magnetic resonance contrast agent. Nat Med. 2011; 17:383–8. [PubMed: 21336283]
31. von Bary C, Makowski M, Preissel A, Keithahn A, Warley A, Spuentrup E, Buecker A, Lazewatsky J, Cesati R, Onthank D, Schickl N, et al. MRI of coronary wall remodeling in a swine model of coronary injury using an elastin-binding contrast agent. Circ Cardiovasc Imaging. 2011; 4:147–55. [PubMed: 21378029]
32. Phinikaridou A, Andia ME, Indermuehle A, Onthank DC, Cesati RR, Smith A, Robinson SP, Saha P, Botnar RM. Vascular remodeling and plaque vulnerability in a rabbit model of atherosclerosis: comparison of delayed-enhancement MR imaging with an elastin-specific contrast agent and unenhanced black-blood MR imaging. Radiology. 2014; 271:390–9. [PubMed: 24475852]
33. Sahul ZH, Mukherjee R, Song J, McAteer J, Stroud RE, Dione DP, Staib L, Papademetris X, Dobrucki LW, Duncan JS, Spinale FG, et al. Targeted imaging of the spatial and temporal variation of matrix metalloproteinase activity in a porcine model of postinfarct remodeling: relationship to myocardial dysfunction. Circ Cardiovasc Imaging. 2011; 4:381–91. [PubMed: 21505092]
34. Li SH, Sun Z, Guo L, Han M, Wood MF, Ghosh N, Vitkin IA, Weisel RD, Li RK. Elastin overexpression by cell-based gene therapy preserves matrix and prevents cardiac dilation. J Cell Mol Med. 2012; 16:2429–39. [PubMed: 22435995]

Europe PMC Funders Author Manuscripts

Clinical Summary

Here, we developed a new multi nuclear MRI imaging protocol that allows visualising and quantifying myocardial inflammation and ECM remodelling simultaneously in a murine model of permanent coronary occlusion. The imaging approach is based on $^{19}F/^{1}H$ multinuclear MRI in concert with fluorine nanoparticles and an elastin specific MR contrast agent (Gd-ESMA). This is the first study that assessed inflammation and ECM remodelling simultaneously with a single non-invasive imaging modality and could provide important insights in post infarct remodelling in patients developing heart failure. We also demonstrated the prognostic value of quantifying inflammation and ECM remodelling 7 days post MI. A well-balanced inflammatory response was beneficial for maintaining left ventricular function while extensive ECM remodelling was detrimental. If translated into the clinic, this work could provide clinicians with a new tool to non-invasively assess inflammation and ECM remodelling (focal and diffuse fibrosis), which is not possible with currently available contrast agents or non-contrast enhanced imaging methods. In summary, we demonstrated the feasibility of measuring myocardial inflammation and ECM remodelling (fibrosis) non-invasively, two key processes in tissue injury, and has great potential beyond cardiac imaging such as for the assessment of renal, liver or lung inflammation and fibrosis.

Europe PMC Funders Author Manuscripts

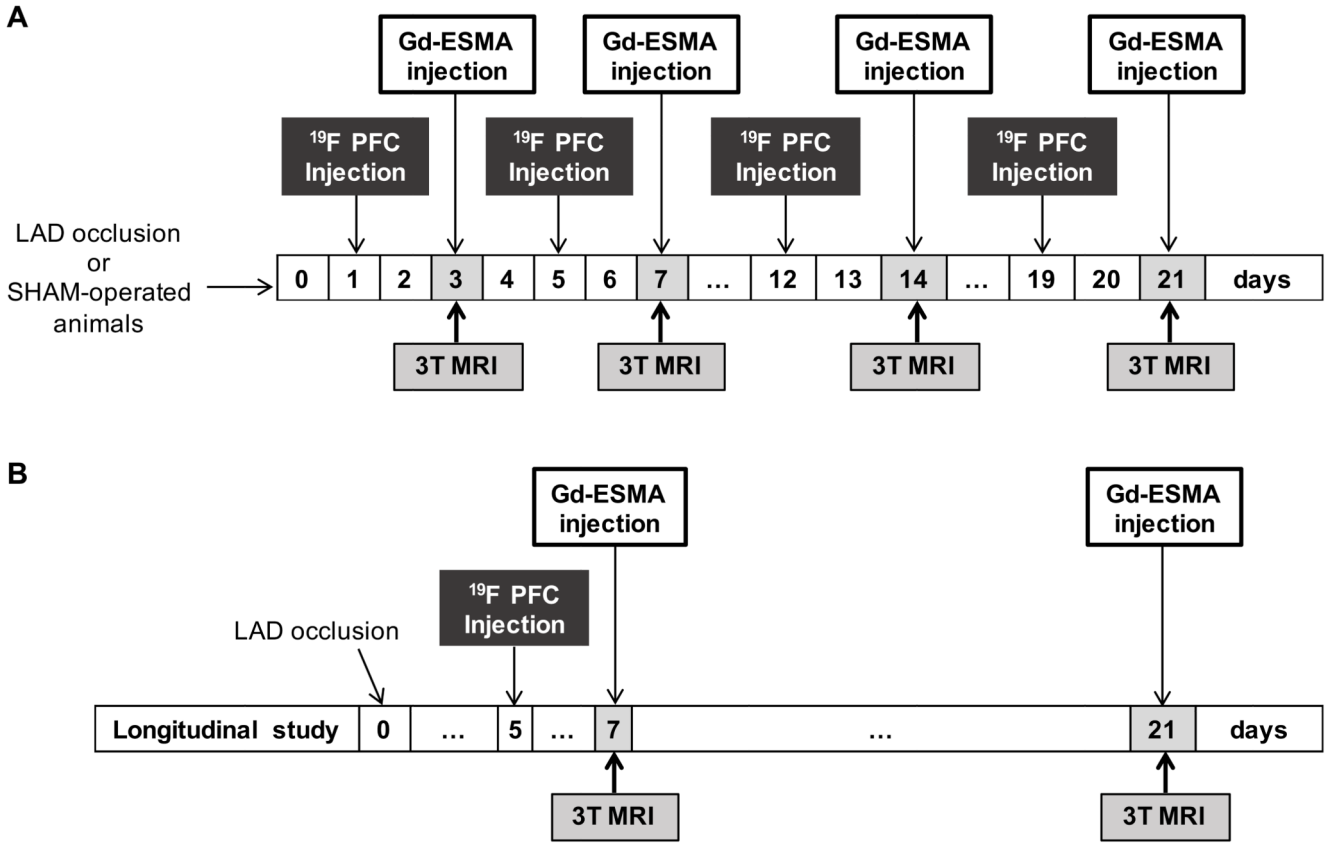

Figure 1.

Experimental study design. Myocardial infarction was induced in C57Bl6 female mice after permanent occlusion of the left anterior descending coronary artery (LAD). MRI scans were performed after intravenous injection of ^{19}F PFCs and Gd-ESMA, 48 and 1h before imaging sessions, respectively. (A) Mice (n=8 per group/time point) were imaged at 3, 7, 14 and 21 days post-MI. SHAM-operated mice (n=6 per group/time point) were imaged at the same time-points and were used as controls. At the end of the scans, mice were culled and hearts were extracted for histology and NMR (n=4/group and 3-SHAM-operated animals/time-point for each technique) (B) 15 mice were imaged longitudinally at 7 and 21 days post-MI. MRI, magnetic resonance imaging; ^{19}F PFC, ^{19}F perfluoro-15-crown-ether emulsions; Gd-ESMA, elastin/tropoelastin specific MR contrast agent.

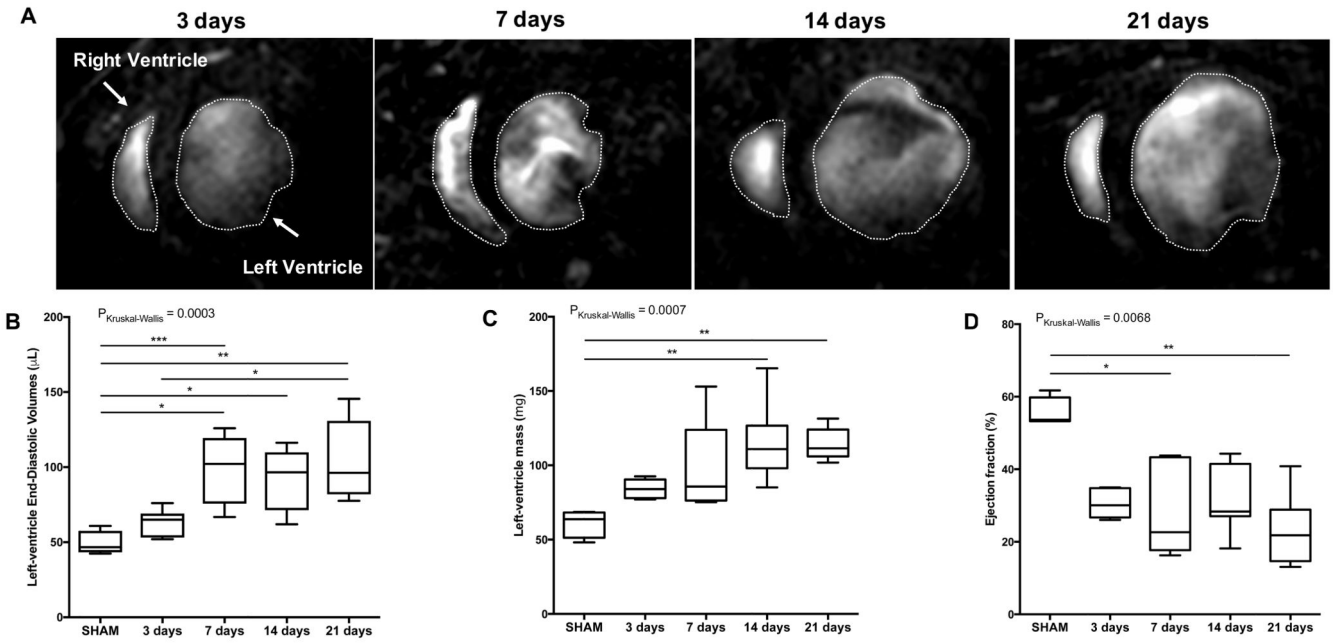

Figure 2.

Functional and volumetric parameters of the heart at 3,7,14 and 21 days post-MI and SHAM-operated mice. (A) Representative anatomical short-axis images of the heart. Myocardium is depicted in orange; the star indicates myocardial wall thinning at day 21. (B) Left ventricular end-diastolic volume progressively dilates from acute to late stages of MI. (C) Increasing Left ventricular mass and (D) decreasing Ejection fraction were observed over time. N=8 MI animals/time-point, N=4 SHAM-operated animals/time-point. MI: myocardial infarction. *P<0.05, **P<0.01.

Europe PMC Funders Author Manuscripts

Europe PMC Funders Author Manuscripts

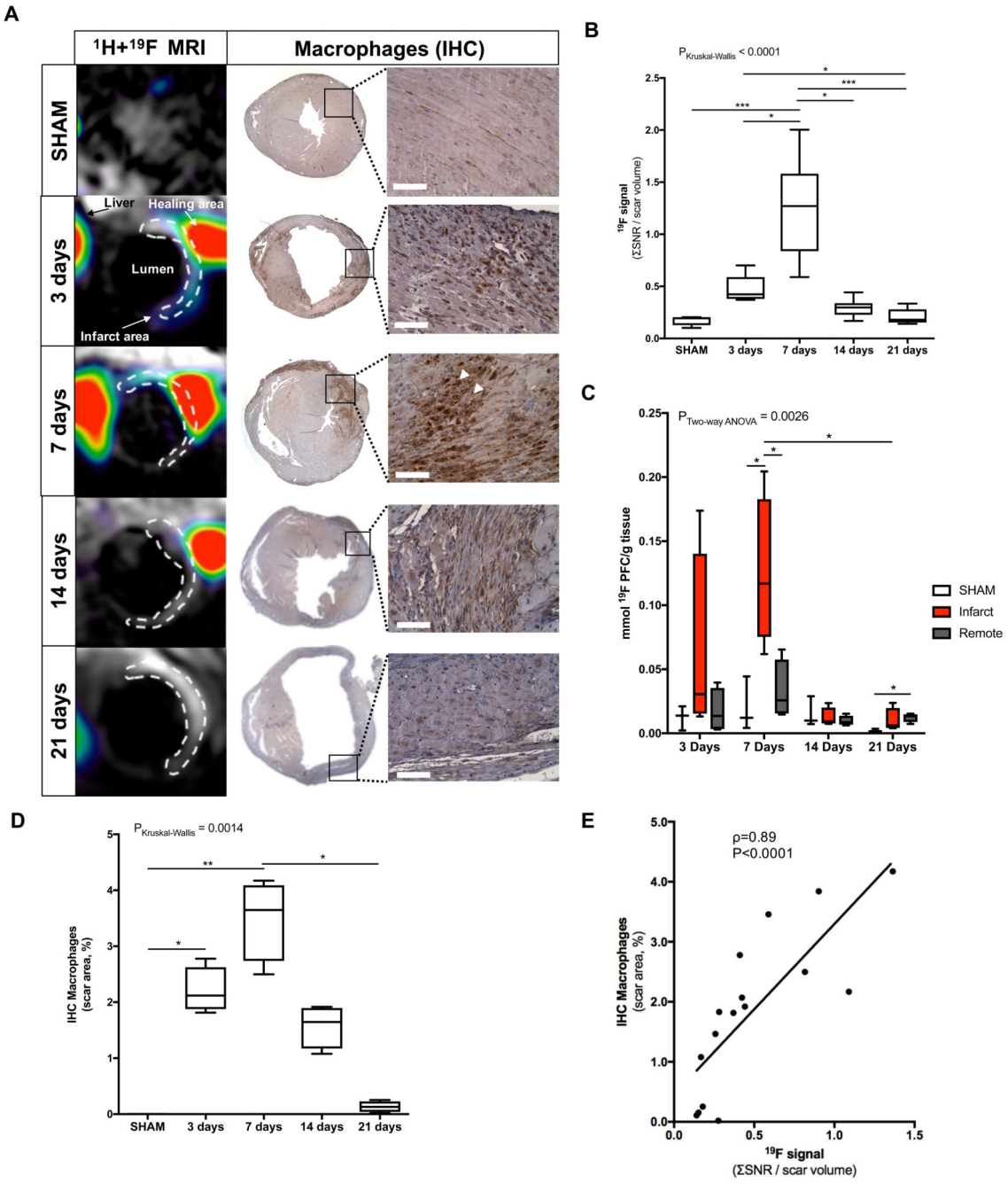

Figure 3.

Assessment of inflammatory response after myocardial infarction in mice at 3T MRI using ^{19}F perfluorocarbons. (A) Representative short-axis views of co-registered ^{1}H+^{19}F images (left column; N=8 MI animals/time-point, N=6 SHAM-operated animals/time-point) and macrophage IHC (macrophages identified as MAC-3 positive, brown. N=4 MI animals/timepoint, N=3 SHAM-operated animals/time-point) from the heart at 3, 7, 14 and 21 days after MI. (B) *In vivo* ^{19}F MRI signal quantification. (C) *Ex vivo* ^{19}F NMR signal quantification (N=4/timepoint, N=3 SHAM-operated animals). (D) IHC macrophages

quantification shown a significantly decrease between 7 and 21 days after infarct. (E) Correlation between *ex vivo* macrophages IHC and *in vivo* ^{19}F MRI signal. Spearman correlation (N=20, ρ=0.89, P<0.0001). IHC:immunohistochemistry. Scale bar, 50μm. *P<0.05,**P<0.01,***P<0.001.

Europe PMC Funders Author Manuscripts

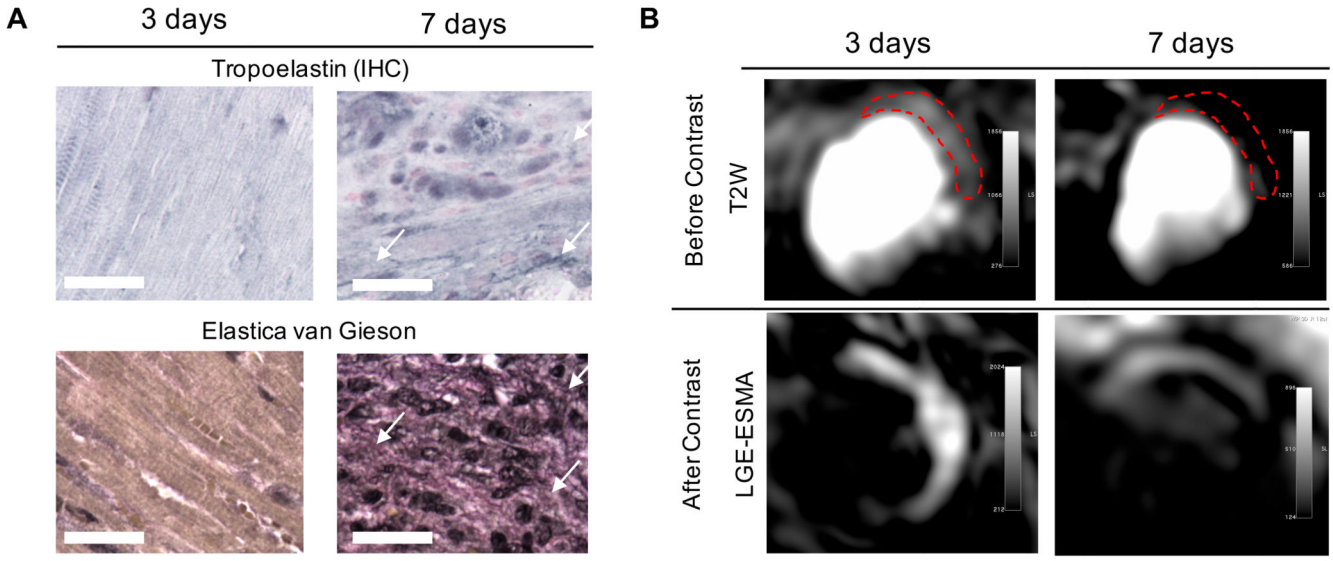

Figure 4.

Assessment of elastin/tropoelastin and myocardial edema in mice with myocardial infarction. (A) Tropoelastin IHC and Elastica van Gieson (black staining) reveal the absence of protein deposition within the heart at 3 days, starting to accumulate at day 7 (arrows). (B) T_2-weighted images showing high signal intensity on the lateral wall (top images); Contrast-enhanced image (late gadolinium enhancement) showing high signal intensity in the infarcted areas (middle images). IHC:immunohistochemistry. Scale bar, 25μm.

Europe PMC Funders Author Manuscripts

Europe PMC Funders Author Manuscripts

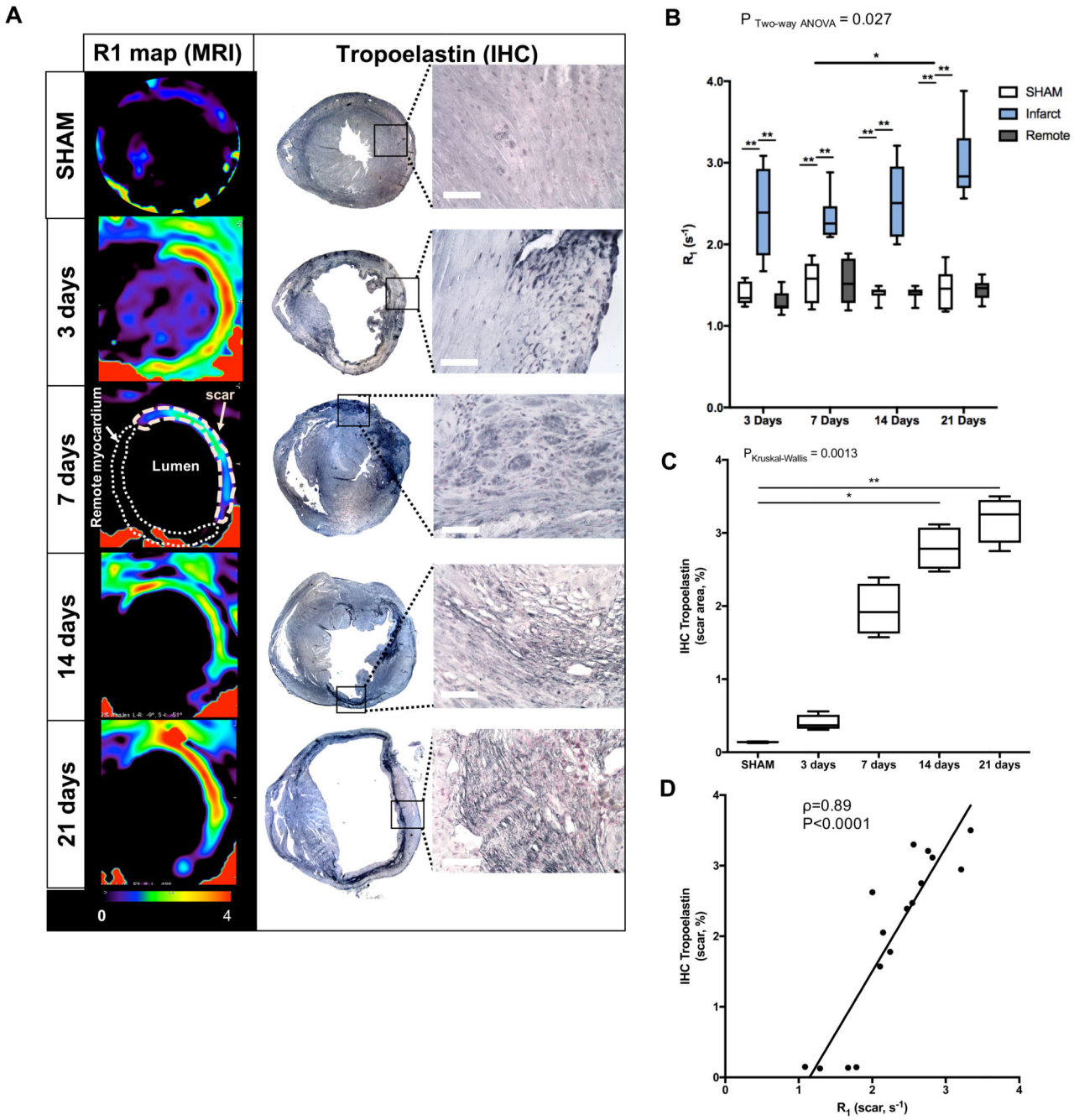

Figure 5.

***In vivo* imaging of extracellular matrix remodeling after myocardial infarction with a gadolinium-based elastin/tropoelastin-specific contrast agent.** (A) Representative short-axis images of relaxation rate (R_1, left columns) maps and tropoelastin IHC (right columns) of the hearts sections at 7, 14 and 21 days post-MI at 3T MRI. Tropoelastin fibers were identified as black fine fiber network. (B) Quantification of the R_1 in the infarct, remote myocardium (N=8/time-point) and in SHAM-operated animals (N=6 per time-point). R_1 values increased significantly from 7 to 21 days post-MI. (C) IHC quantification, showing a

significantly increase in tropoelastin fibers from 7 to 21 days post-MI (N=4/time point. N=3 SHAM, PKruskal-Wallis SHAM vs 21days<0.01). (D) Correlation between *ex vivo* measurements of tropoelastin IHC and *in vivo* R_1 values of the scar. Spearman correlation (N=16, ρ=0.89, P<0.0001). IHC:immunohistochemistry. Scale bar, 50μm. *P<0.05,**P<0.01,***P<0.001.

Europe PMC Funders Author Manuscripts

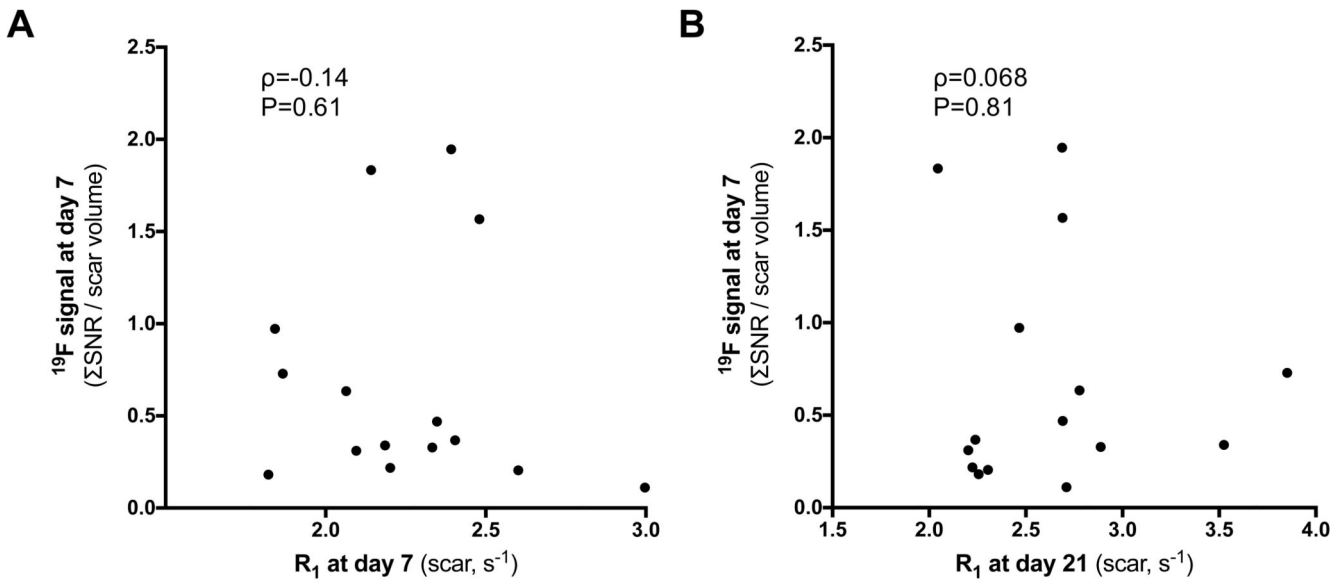

Figure 6.

There is no correlation between ^{19}F signal at day 7 and (A) Gd-ESMA uptake 7 days after MI and (B) Gd-ESMA uptake in the infarcted myocardium at day 21 post-MI.

Europe PMC Funders Author Manuscripts

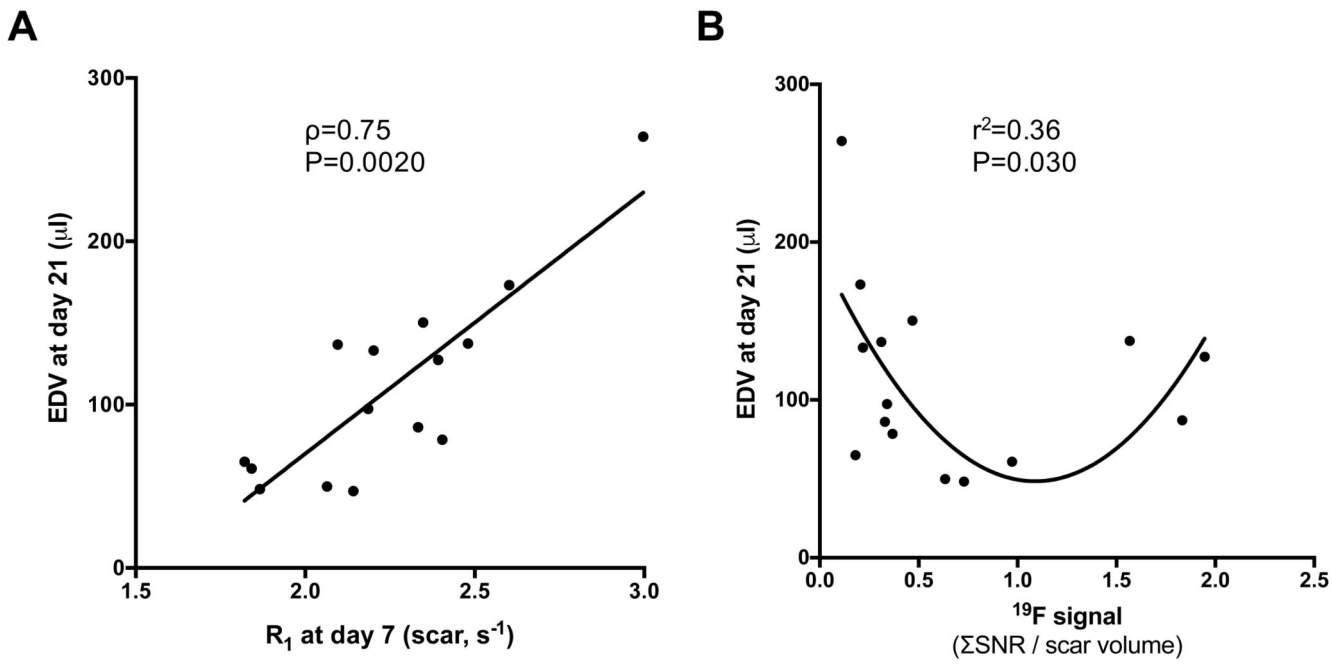

Figure 7.

Correlation between EDV at day 21 and R1 values and ^{19}F signal at day 7. (A) Linear correlation was found between EDV and R_1 (Gd-ESMA uptake), (B) Quadratic regression was found between EDV and ^{19}F SNR.

Europe PMC Funders Author Manuscripts